# ON CHARGED PARTICLE TRACKS IN CELLULOSE NITRATE AND LEXAN*

by

E. V. Benton and R. P. Henke

July 1972



DEPARTMENT OF PHYSICS
UNIVERSITY OF SAN FRANCISCO

# ON CHARGED PARTICLE TRACKS IN CELLULOSE NITRATE AND LEXAN*

by

E. V. Benton and R. P. Henke

July 1972

Interim Technical Report

No. 19

Department of Physics

University of San Francisco

San Francisco, California 94117

*Work sponsored by NASA, G. C. Marshall Space Flight Center, Alabama, under contract NAS8-26758.

ABSTRACT*

Investigations have been performed aimed at developing plastic nuclear track detectors into precise and quantitative tools for recording and measuring multicharged, heavy particles. Accurate track etch rate measurements as a function of LET have been performed for cellulose nitrate and Lexan plastic detectors. This was done using a variety of incident charged particle types and energies. The effect of aging of latent tracks in Lexan in different gaseous atmospheres has been investigated. Range distributions of high energy $^{14}N$ particle Bevatron beams in nuclear emulsion were measured. Investigation of charge resolution and Bragg peak measurements were carried out using plastic nuclear track detectors.

*The track geometry portion of this report was previously published in Nuclear Instruments and Methods 97 (1971) 483-489.

## INTRODUCTION

The purpose of this effort was to carry out investigations aimed at refining the techniques and methods of plastic nuclear track detectors.[1,2] The goal is to develop plastic nuclear track detectors into precise and quantitative tools for heavy particle measurements. Some of the areas investigated include: The behavior of the track etch rate $V_T$, as a function of particle LET in Lexan and cellulose nitrate, the response of different types of cellulose nitrate as well as of the different surfaces of a single sheet of the same material, the response as a function of the etching time, and the aging effect of the latent tracks as a function of storage atmosphere. An analysis of the response of cellulose nitrate and Lexan is also given. Finally, the detectors were utilized in practical applications involving the test of charge resolution and the measurement of the Bragg peak of multicharged, high energy particle beams from the Bevatron.

## CELLULOSE NITRATE

A stack of cellulose nitrate layers of the type USF #4 was exposed to a stopping beam of $^{16}O$ particles at the Berkeley Bevatron. The individual detector layers were etched at 40°C in 6.25 N NaOH solution without stirring. Two etch times were used, 5.0 and 20.0 hours. Measurements of the track etch rate, $V_T$, were performed on both sets of layers and for both surfaces of each detector sheet. The results are shown in Figures 1, 2 and 3. Here $V_T$ in microns per hour is plotted against the particle residual range in microns. It is observed that on a log - log plot, the data is well-approximated by a straight line in each of the cases.

In Figure 1 is shown the $V_T$ measurements for both the "air" and the "metal" surface of the detector. This refers to the casting process for preparing cellulose nitrate where a nitrocellulose solution is poured into a metal pan and is then allowed to dry. It is observed that for a 5.0 hour etch, the data from both surfaces join smoothly together.

The $V_T$ data for the 20.0 hr. etch is given in Figures 2 and 3. Intercomparisons with the data for the 5.0 etch shows that the "air surface" data for the 20.0 hr. etch fits well together with both sets of data for the 5.0 etch. However, the "metal surface" data for the 20.0 hr. etch is measurably different from the other three sets. This difference suggests a sensitivity difference between the two plastic surfaces. Apparently, there is a gradual surface-to-surface transition in the properties of the cast material which becomes more pronounced with increasing etch times. These observations were further substantiated by an even longer etch time of 100 hr. Here, large differences in the track structure between the two surfaces was noted.

The track etch rate as a function of residual range was also measured in USF #3 cellulose nitrate, using samples exposed at the PPA to high energy beams of $^{20}Ne$ particles. This detector is similar to USF #4 type, however, is slightly less sensitive. The track etch rates were measured on one layer. The tracks due to the particles were then traced to their stopping points to find the residual range that applied for the measured etch rate. A total of 48 tracks were traced through, and four layers were required to reach the stopping points of all of the particles. Because of the non-uniform thickness of the CN layers, the thickness of each layer at the point of passage of each particle had to be measured.

The results are shown in Figure 4. The track etch rate, $V_T$, is plotted as a function of the particle residual range, R. The etch rate calibration obtained by drawing a straight line on this log - log plot through the top group of tracks which are assumed to be $^{20}Ne$ particles is

$$V_T = 3083\ LET^{3.626},$$

where $V_T$ is in μ/hour and LET is $LET_{350}$ in MeV/μ. Using this calibration, the dashed curves shown were drawn for the isotopes indicated.

It can be seen that the measured points fall nicely into two groups. The logical charge assignment for the upper and most populated group is the nominal beam ion, $^{20}Ne$. From this assumption and the calibration curve drawn through this group of points, the dashed curves follow. It is assumed that the ions represented by the other groups of points are produced through nuclear interactions of the incident $^{20}Ne$ beam. For this reason it is not surprising to find some of the points not falling on the dashed line corresponding to the most abundant isotope in nature.

The range of track etch rates measureable in this case is largely governed by the constant etch time of the detector used for these measurements. A longer etch time would have allowed the measurement of much lower etch rates, and a shorter etch time would have allowed the measurement of somewhat greater etch rates. The same calibration would not necessarily follow, however. This is because 1) the etch rate calibration can only be expected to be represented by a power function in LET over a limited range of LET values, and 2) the etch rate is a function of the etch time because it varies with the depth in the sample.

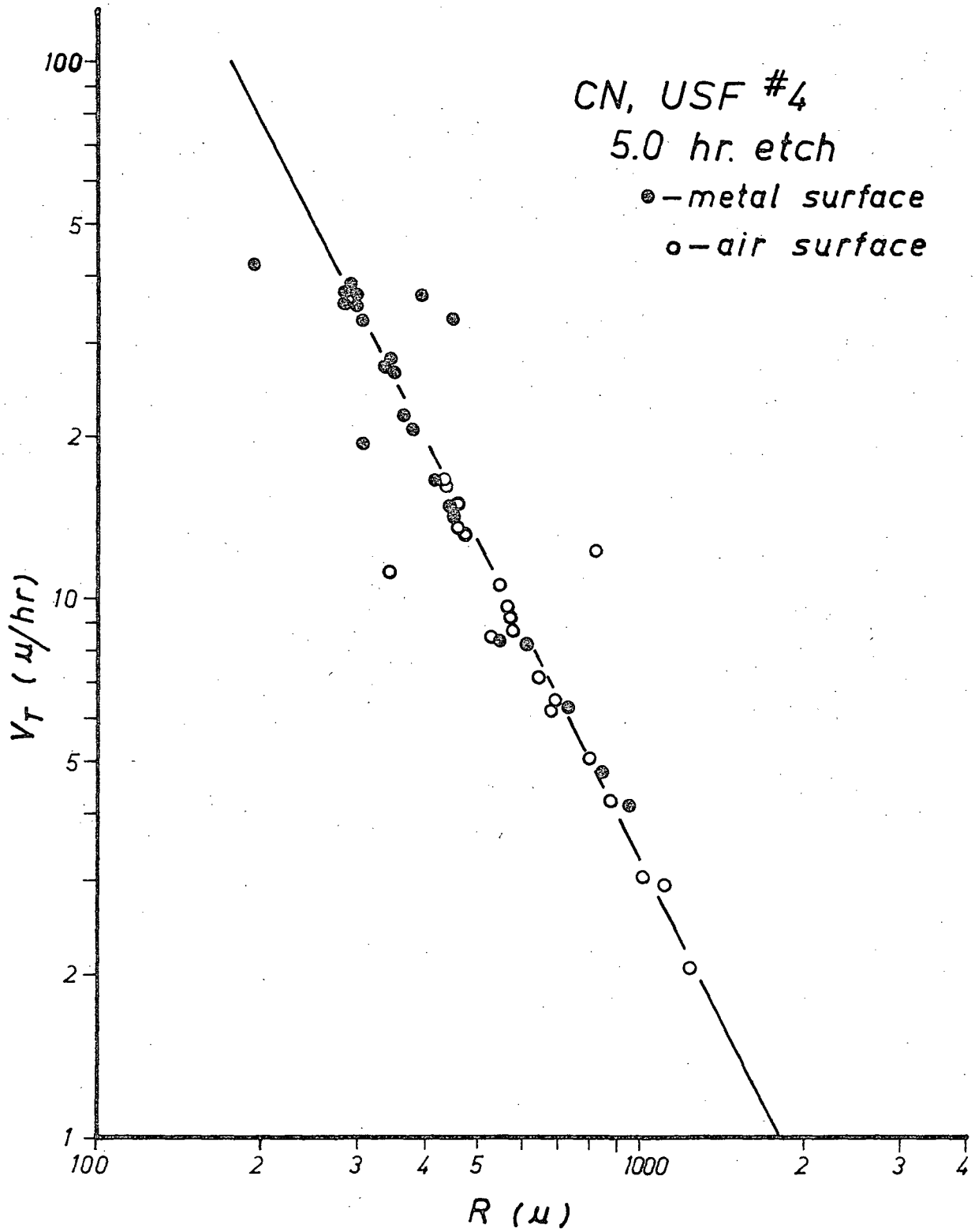
CN, USF #4
5.0 hr. etch
●–metal surface
o–air surface
100
5
2
10
5
2
1
$V_T$ (μ/hr)
100
2
3
4
5
1000
2
3
4
R (μ)

Figure 1

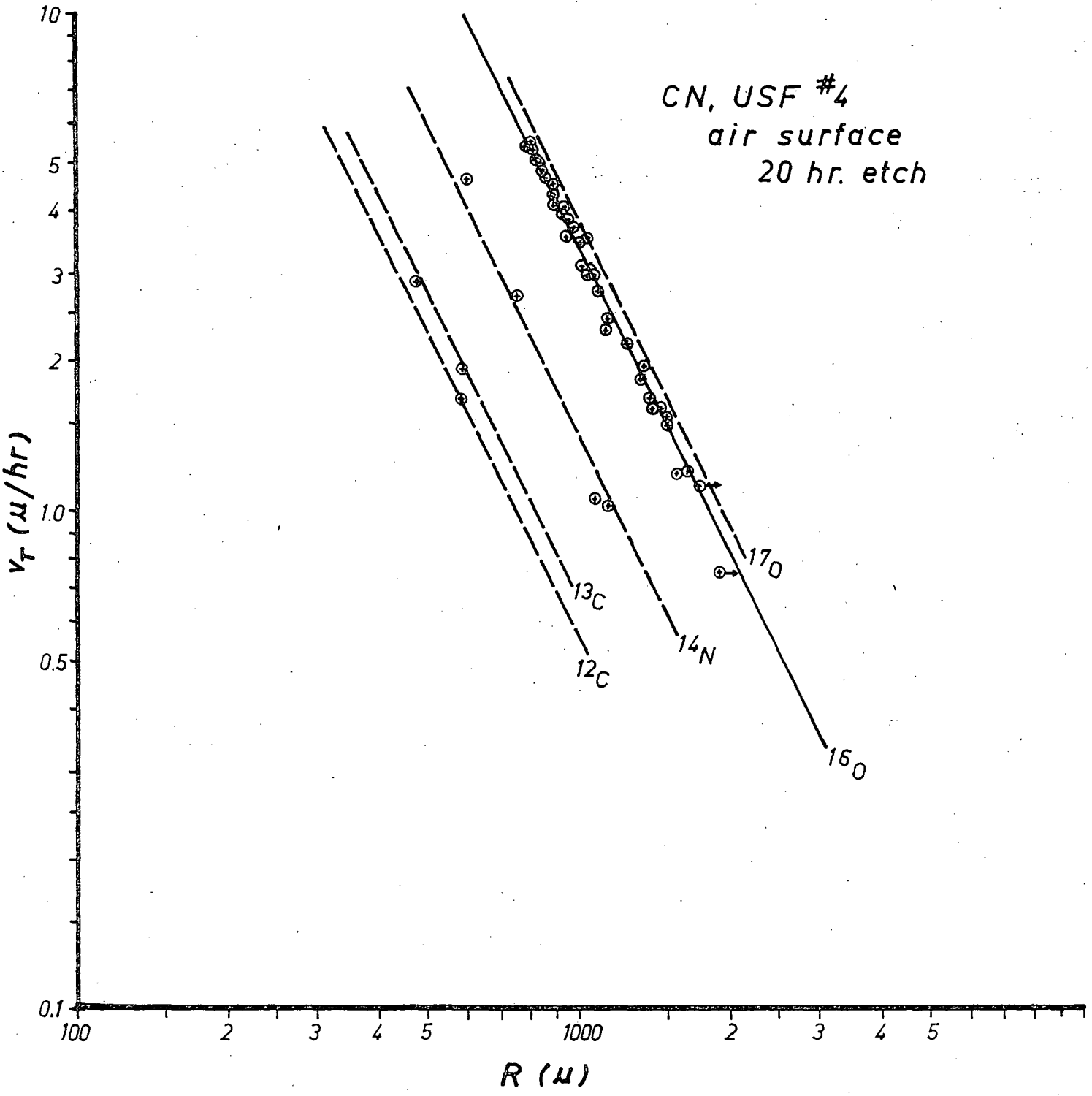
CN, USF #4
air surface
20 hr. etch
$v_T$ (μ/hr)
R (μ)
10
5
4
3
2
1.0
0.5
0.1
100
2
3
4
5
1000
2
3
4
5
$^{13}C$
$^{12}C$
$^{14}N$
$^{17}O$
$^{16}O$

Figure 2

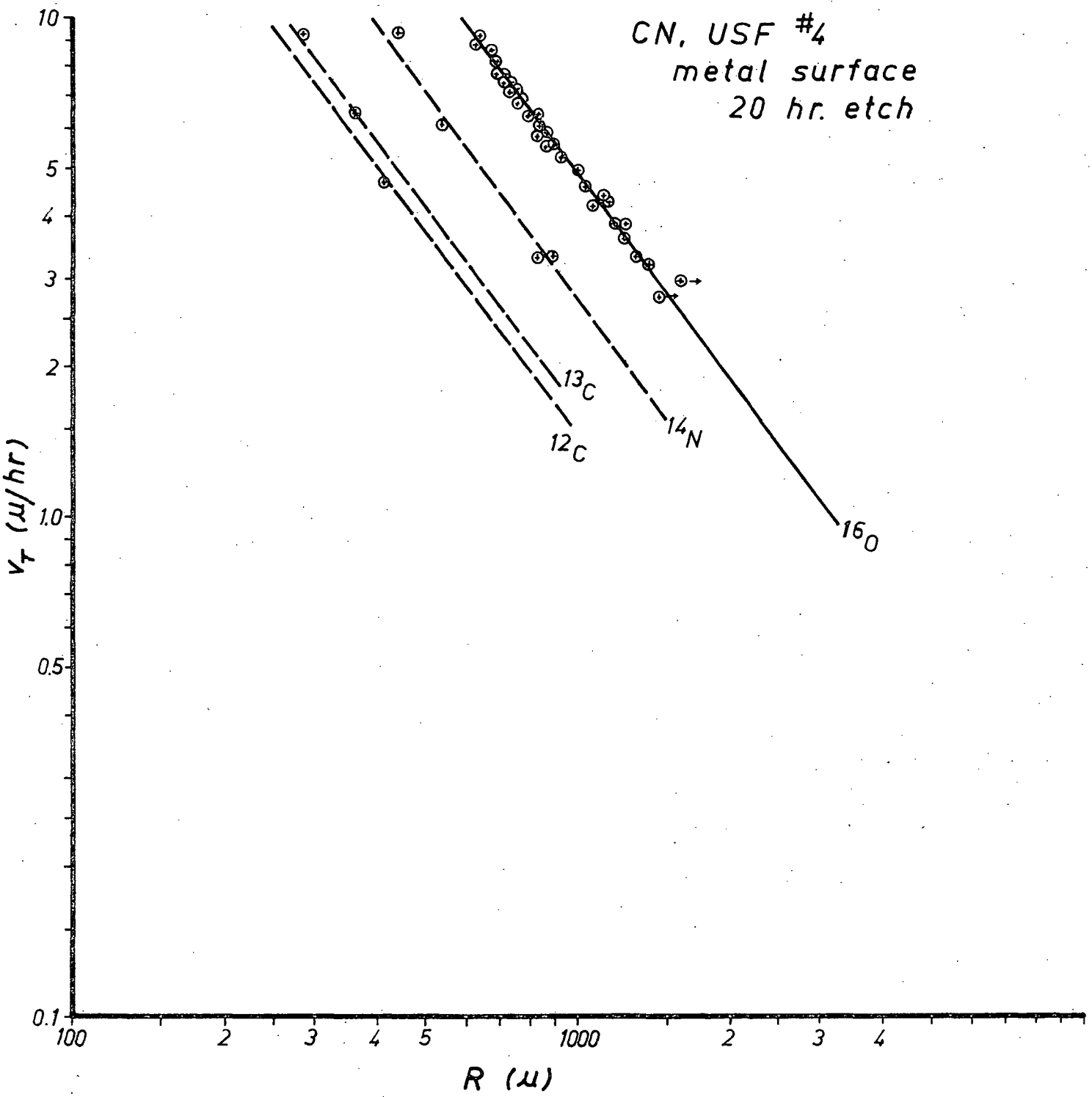
CN, USF #4
metal surface
20 hr. etch
$^{12}C$
$^{13}C$
$^{14}N$
$^{16}O$
$v_r$ (μ/hr)
R (μ)
10
5
4
3
2
1.0
0.5
0.1
100
2
3
4
5
1000
2
3
4

Figure 3

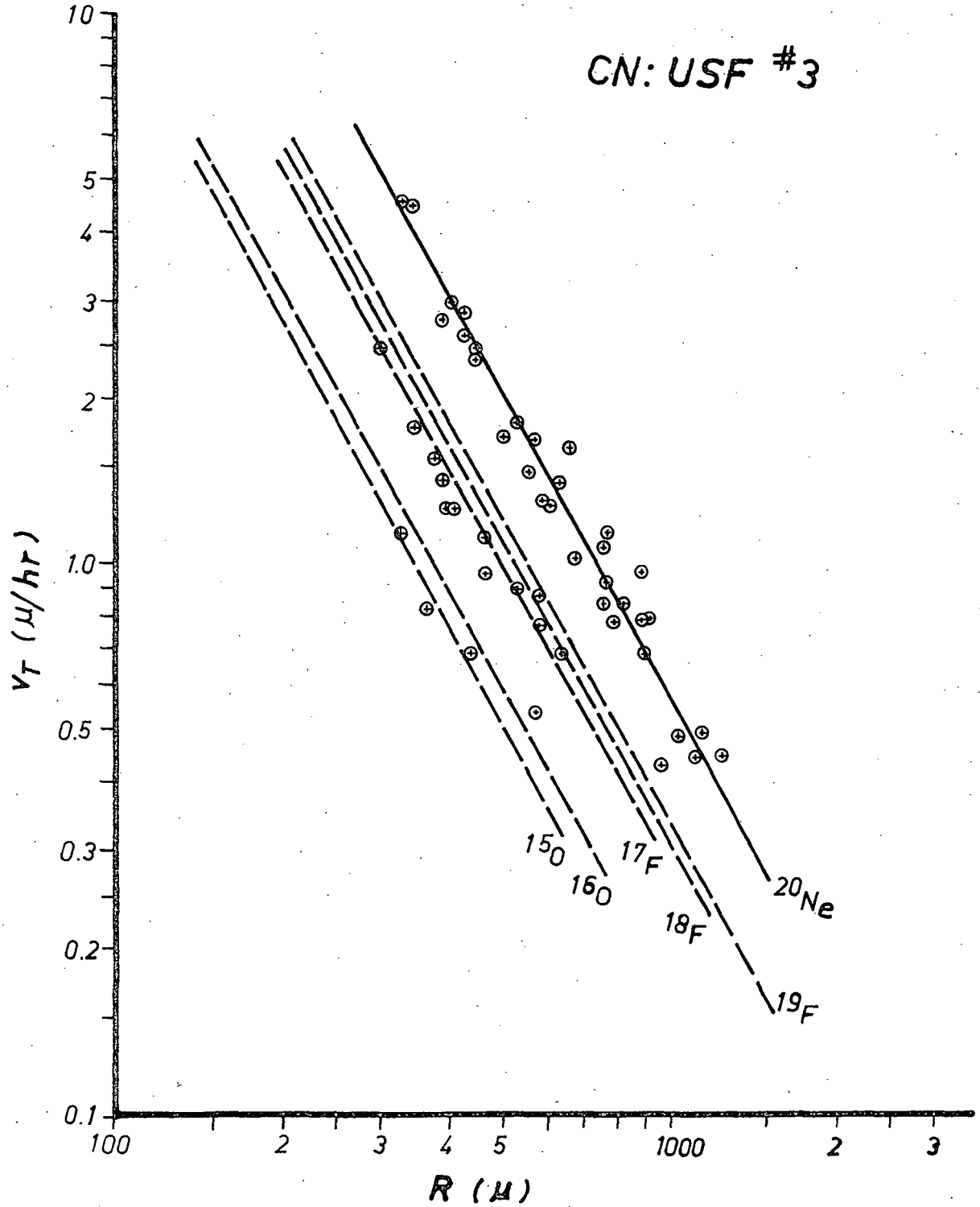
CN: USF #3
10
5
4
3
2
1.0
0.5
0.3
0.2
0.1
$v_T$ (μ/hr)
100
2
3
4
5
1000
2
3
R (μ)
$^{15}O$
$^{16}O$
$^{17}F$
$^{18}F$
$^{19}F$
$^{20}Ne$

Figure 4

## LEXAN

It is well known that latent tracks in plastic nuclear track detectors are affected by various environmental parameters such as UV light, oxygen in the atmosphere, etc.[3] A study was performed to determine the affect of storage of latent tracks in Lexan stored in various gaseous atmospheres including $O_2$, $N_2$ Ar, $CO_2$ and vacuum. Samples of Lexan exposed to 10.1 MeV/nucleon $^{40}Ar$ ions were stored in the various atmospheres, in the dark, and then processed at various intervals of time. The results are shown in Figure 5. As is observed, samples stored in inert atmospheres of $N_2$, $CO_2$ and Ar showed no measurable change in $V_T$. Samples stored in vacuum showed a definite decrease in $V_T$ with storage time. A sample stored in air at 0°C in the dark showed no measurable increase in $V_T$ even after a 1,000 day storage period.

Measurements of UV-irradiated Lexan were made using stopping $^{16}O$ particle beam of the Bevatron. An UV-irradiation of 32 hours on each side (16-32-16 hours per side) was carried out using a 1,000 watt GE mercury arc lamp at a distance of 12 cm from the arc. The results are given in Figures 6, 7 and 8. It is observed that again the data are well-approximated by a straight line on a log - log plot. In this case, all the data join smoothly together. While a greater variation is observed in the response over a single surface, as compared with, for example, USF #4 cellulose nitrate, a much smaller variation in response is observed from one surface of the detector to the next. It should be pointed out that some of the scattering of the data is the result of

measurements of tracks due to secondaries stopping in the detector which were produced by the interaction of the primary beam with the stopping material.

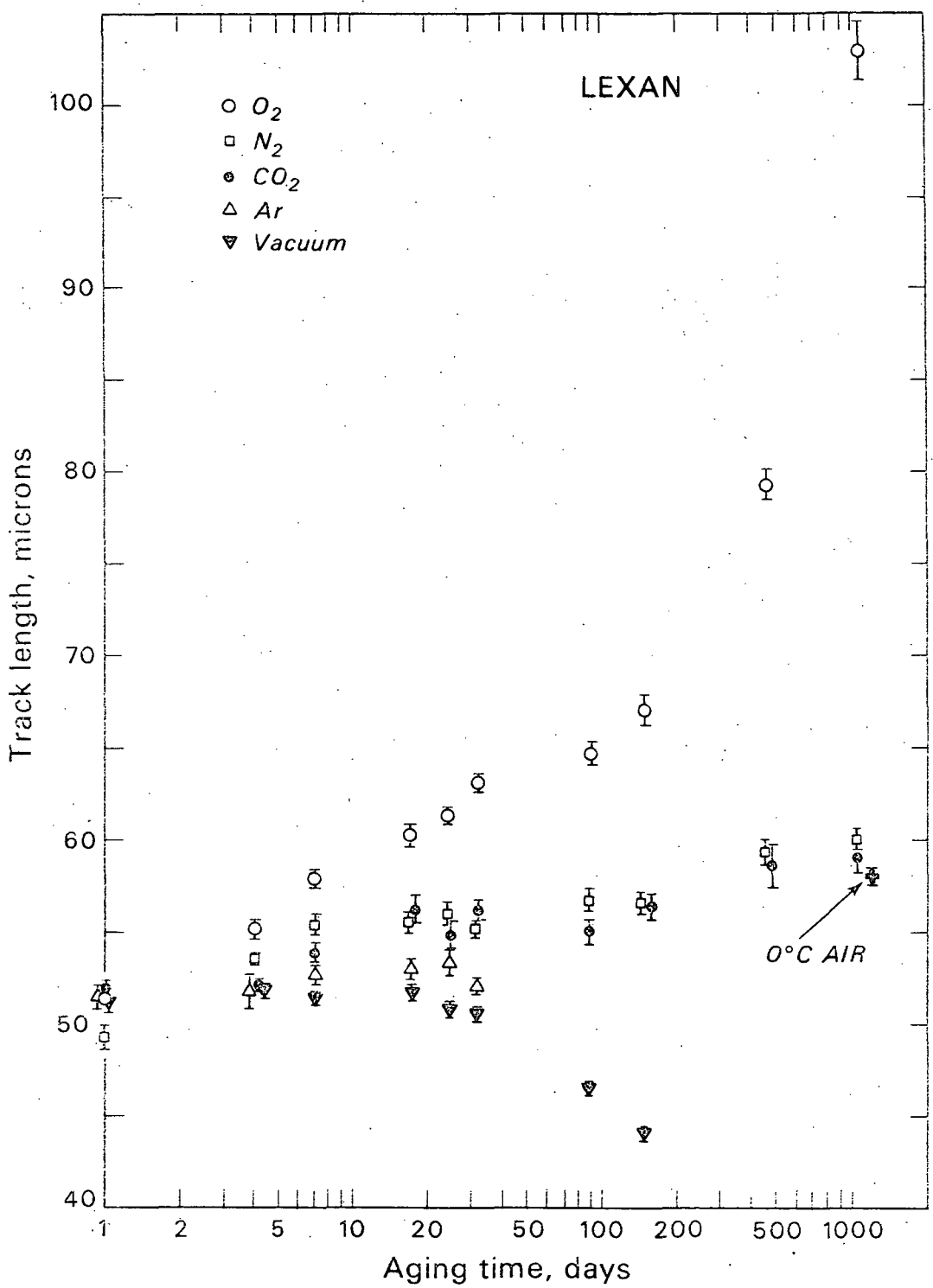
LEXAN
O2
N2
CO2
Ar
Vacuum
0°C AIR
Track length, microns
Aging time, days
100
90
80
70
60
50
40
1
2
5
10
20
50
100
200
500
1000

Figure 5

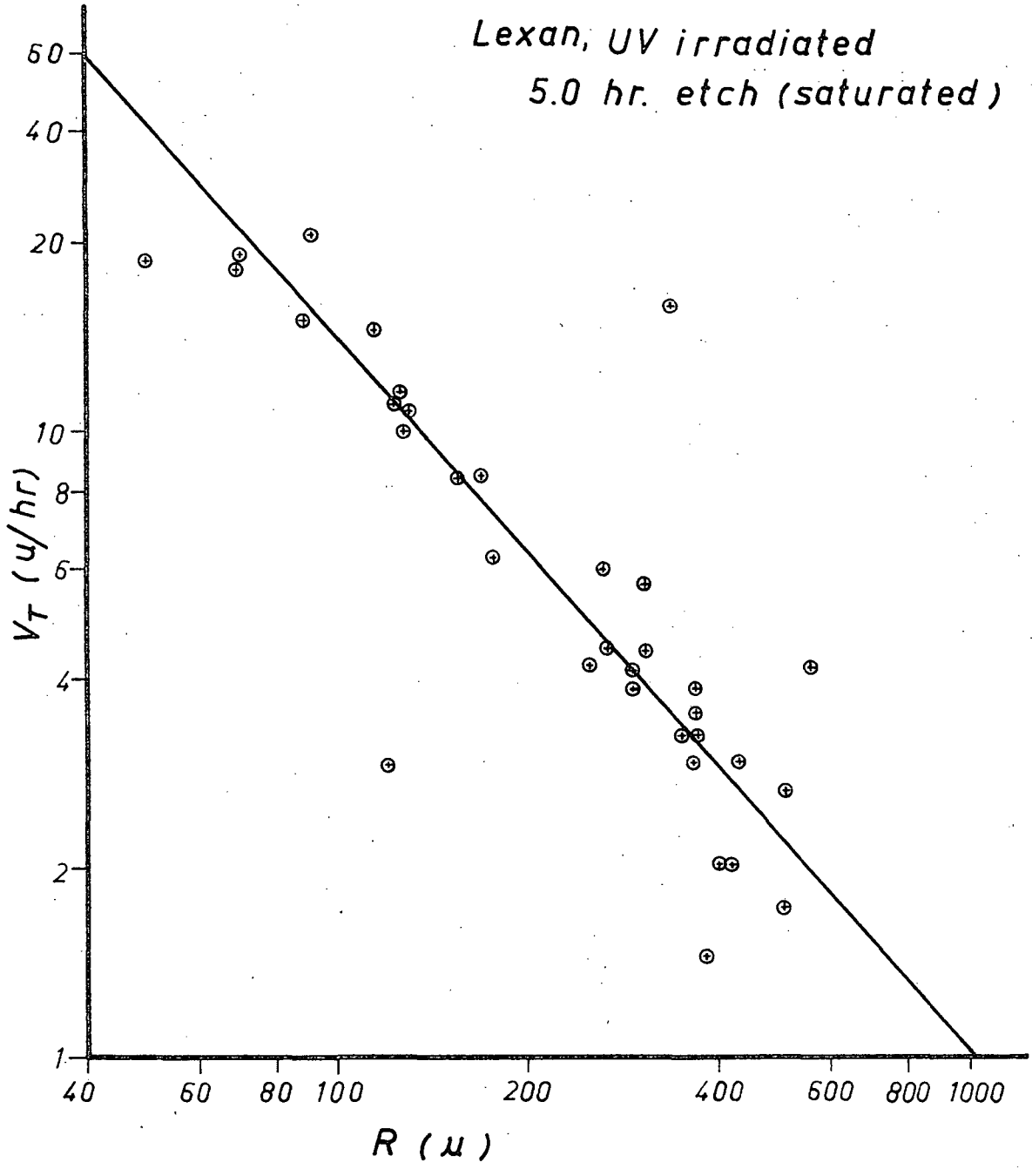
Lexan, UV irradiated
5.0 hr. etch (saturated)
60
40
20
10
8
6
4
2
1
$V_T$ (u/hr)
40
60
80
100
200
400
600
800
1000
R (u)

Figure 6

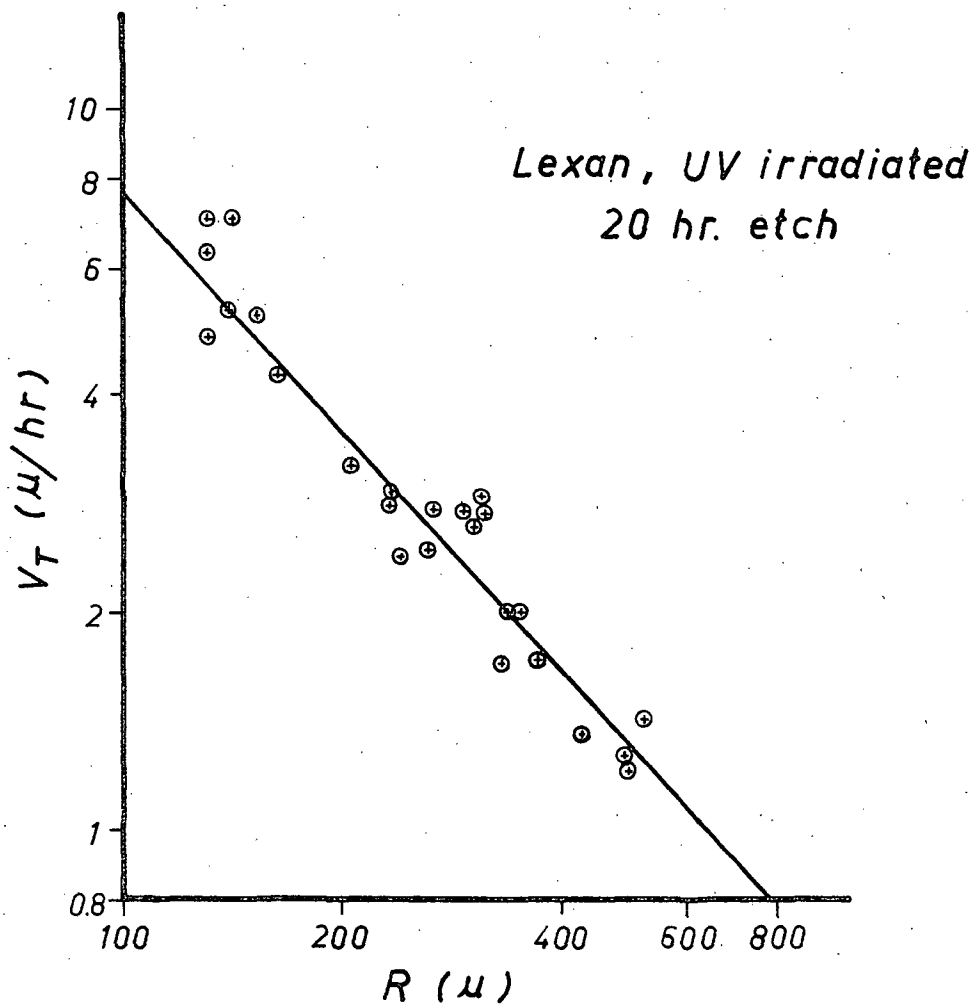
Lexan, UV irradiated
20 hr. etch
10
8
6
4
2
1
0.8
$V_T$ (μ/hr)
100
200
400
600
800
R (μ)

Figure 7

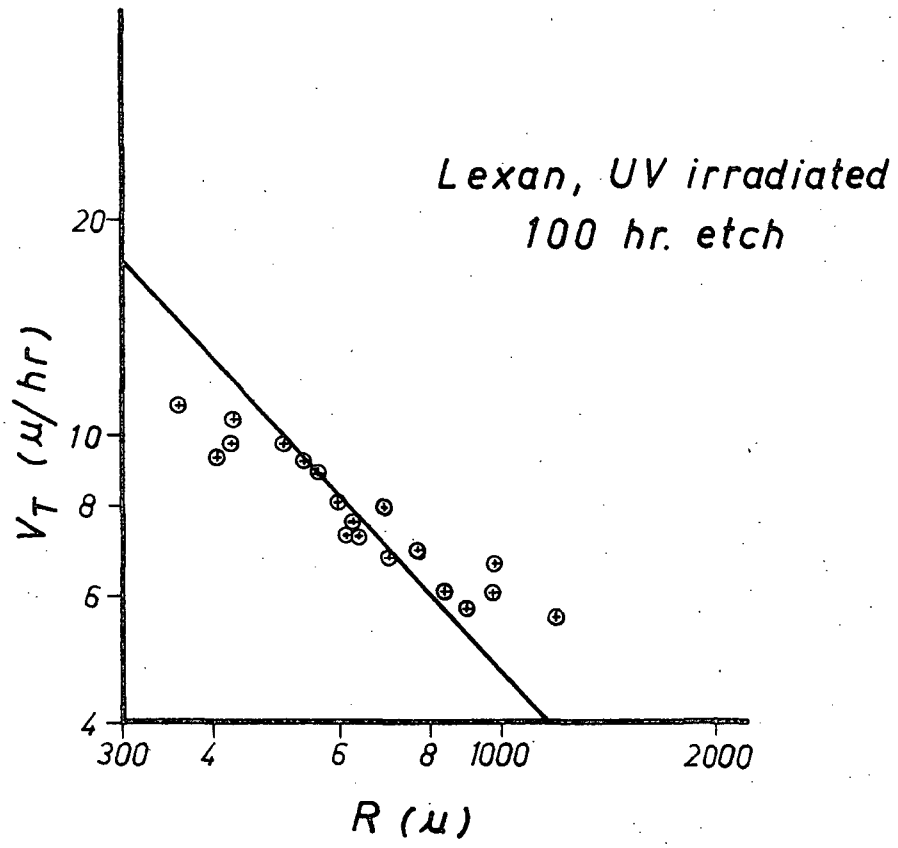
Lexan, UV irradiated
100 hr. etch
20
10
8
6
4
$V_T$ (μ/hr)
300
4
6
8
1000
2000
R (μ)

Figure 8

## COMPARISON OF RESPONSE: CELLULOSE NITRATE AND LEXAN

Plastic nuclear track detectors such as cellulose nitrate, UV irradiated Lexan, and non-irradiated Lexan differ not only in sensitivity but also in the manner in which the etch rate, $V_T$, varies as a function of particle LET. Two detectors may be comparable in sensitivity but because of the differences in the response would be useful in the measurement of different portions of the particle LET spectrum. In this section, the response curves are compared for one type of cellulose nitrate, USF#3, and UV irradiated as well as non-irradiated Lexan.

The basic expression of the etch rate response function of a detector is the track etch rate as a function of the particle $LET_{350}$. Here it is assumed that 350 eV is the proper value $\omega$ for $V_T(Z,A,E) = V_T(LET_\omega)$ where $LET_\omega(Z,A,E)$. A somewhat better parameter than the track etch rate is the normalized track etch rate,

$$\nu = \frac{V_T}{V_G}$$

for cellulose nitrate and non-UV irradiated Lexan or

$$\nu = \frac{V_1}{V_{G1}}$$

for UV irradiated Lexan. Here $V_1$ and $V_{G1}$ are the etch rates corrected for UV attenuation. The quantity $\nu$ is more useful than $V_T$ because the ratio of $V_T/V_G$ is the governing factor for both for particle registration ($\nu > \csc \delta$) and measurability of $V_T$ in the region $\nu \gg 1$.

In Figure 9 are shown measurements of $\nu(LET_{350})$ for several different plastic-

processing combinations. The two curves of greatest interest are the USF #3 curve and the UV-irradiated Lexan curve. They cover the greatest range in $\nu (1 < \nu < 200)$. Several comparisons can be made between these two response curves:

1. For all values of $\nu$, $\frac{d \ln \nu}{d \ln LET_{350}}$ is greater for CN than for Lexan. This means the CN gives a much more sensitive measurement of LET. Thus a given percentage accuracy measurement of $\nu$ gives a more accurate value of LET in CN than in Lexan.
2. For the measurable range of $\nu$ $(0 < \nu < 200)$ the range of $LET_{350}$ values for Lexan $(0.1 < LET_{350} < 1.0)$ is much greater than the values for CN. This means that CN is only useful over a much more limited range of $LET_{350}$ values. In fact, as can be seen by the non - UV-irradiated curve, Lexan without UV irradiation can be used to measure greater values of $LET_{350}$ yet. (If the curve is extrapolated, the upper limit of measurable $\nu$ $\sim$200, is reached at $LET_{350} \simeq 2.5$ MeV/$\mu$).
3. $\frac{d^2 \ln \nu}{(d \ln LET_{350})^2}$ $\begin{cases} <0 & \text{CN} \\ >0 & \text{Lexan} \end{cases}$

   This positive curvature of Lexan and negative curvature of CN on the log - log plot implies that CN yields its greatest LET measurement accuracy at low LET and $\nu$ values, and Lexan its greatest accuracy at high LET values. It should be mentioned, however, that the shift in the Lexan curve at about $\nu = 20$ is probably due to the accumulation of etch products in the track becoming important for $\nu \gtrsim 20$. The effect of this saturation is variable, resulting in an actual decrease rather than the

apparent increase in LET measurement accuracy. Except for this variability in the $V_T(LET_{350})$ curve, accuracy with Lexan for $\nu \gtrsim 2$ is comparable to that of CN but just covers a different range of LET.

4. The critical values of $LET_{350}$, $LET_{350}(\nu = 1) = LET_{350,c}$ of Lexan and CN are approximately the same. That is, in a sense, UV-irradiated Lexan is as sensitive as CN. This is only true, however, for $\delta = 90°$ tracks. At $\delta = 90°$, a particle will register to the same value of $LET_{350}$ in UV-irradiated Lexan and CN. The value of $LET_{350}$ cannot be directly compared, however, because the stopping properties of the two materials are different. In CN the critical value of $\beta$ is still greater than in Lexan, indicating a greater sensitivity.

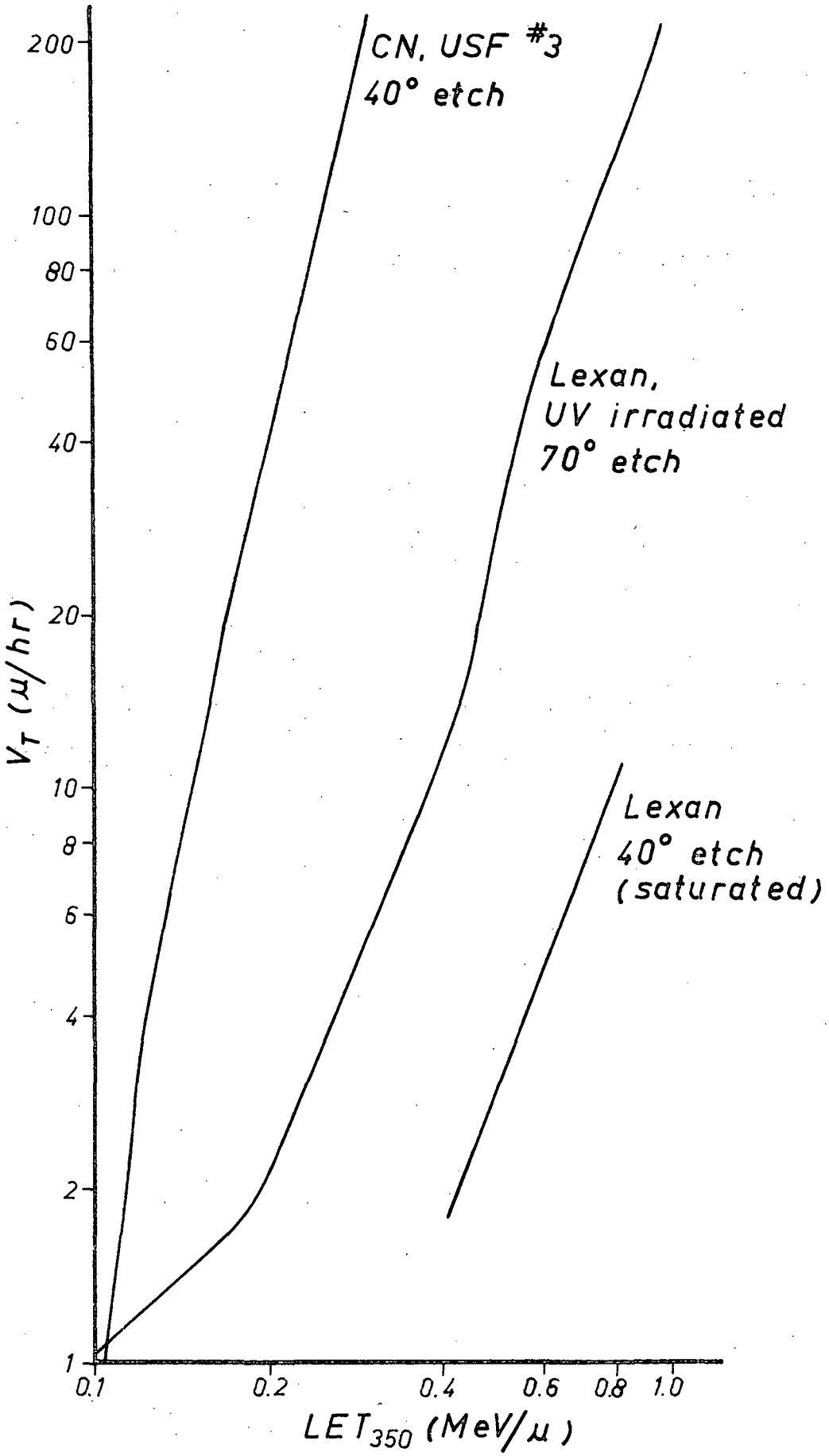
CN, USF #3
40° etch
Lexan,
UV irradiated
70° etch
Lexan
40° etch
(saturated)
200
100
80
60
40
20
10
8
6
4
2
1
$V_T$ (μ/hr)
0.1
0.2
0.4
0.6
0.8
1.0
$LET_{350}$ (MeV/μ)

Figure 6

## COMPARISON OF LEXAN AND CN IN TERMS OF USE

The following discussion still refers to Figure 9 and the remarks of the previous discussion still apply.

1. Z determination

   Both Lexan and CN are useful for Z determination but each has its greatest use in a particular situation. It should be remarked that the basis for all of the discussion in this paper is the assumption of the consistency of the calibration. If tracks of a given LET have very nonreproducible values of $v$, of course the discussion based on the calibration curve is not true for the real situation. The parameter $R_{reg}$ is maximum residual range at which a particle can register.

   a. Particles for which both $V_T$ and R are known.

      In this case a single measurement of $V_T(R)$ gives Z much more accurately in CN (about 5 times more accurately).

   b. $V_T(R)$ measured over entire non-etched-through portion of $R_{reg}$.

      In this situation CN is clearly superior. (1) Fewer values of $V_T(R)$ must be measured. (2) Even with fewer values of $V_T(R)$ measured, at $\delta = 90°$ CN gives $\sim$ 3.6 times the accuracy of Lexan in Z determination. (3) With decreasing dip angles the approximate accuracy of Lexan remains the same, but for CN it increases as $(\sin \delta)^{-0.4}$. (4) The fraction of bulk material to be removed to obtain the greatest accuracy in Z is 0.50 for Lexan but only 0.27 for CN, allowing greater accuracy in $\delta$, and $\alpha$ measurements in CN.

The above discussion assumes equality in the detector thickness for Lexan and CN.

c. Measurements of Z in a relatively thin stack ($<<R_{reg}$) where the particle stopping points are random.

In this situation Lexan has a slight advantage over CN in one respect. Because of the much greater range of LET values measurable, a larger fraction of the registered particles will produce measured Z values than in CN. Many of the tracks in CN will be etched through holes. However, this disadvantage may be offset by the greater stopping density. Thus, the number/$cm^2$ which are not etched through may be the same in CN as in Lexan. Furthermore, for those tracks which are not etched through in CN, the accuracy in Z measurement will be better than in Lexan.

2. Direct measement of the LET spectrum.

Direct measurement of the LET spectrum means measuring $V_T$ and thus LET for each particle track. For this use Lexan is clearly superior because of the greater range of LET that is measurable. In CN only the range $0.1 < LET_{350} < 0.3$ could be measured and even in this case several samples with different etch times would have to be employed. For Lexan the entire range of $0.1 < LET_{350} < 4.0$ could be measured by using different etch times and processing with and without UV. For a single etch time with UV the range of $LET_{350} < 1$. The only advantages offered by CN are better geometry tracks and greater accuracy in the LET measured, but the accuracy of Lexan is quite sufficient.

3. Measurement of particle fluences, LET spectra by track counting, and the "density" parts of the stopping density measurements.

Here CN is clearly superior for several reasons.

a. CN is more sensitive (also greater density, $\rho$, hence greater stopping power per volume) giving greater fluences and better counting statistics.

b. CN is more isotropic in its response. It does not discriminate as strongly as Lexan against the low dip, $\delta$, tracks. Thus when the beam is not isotropic, CN would enable the values of the fluences, LET spectra, and stopping densities as averaged over solid angle to be more closely approximated.

c. The cutoff in etch rate as $R_{reg}$ is approached is much more rapid in CN. This means that the measured track numbers would be much less subject to scanning efficiency variations. A much smaller fraction of the total number of tracks would be of the marginal character.

## HEAVY PARTICLE MEASUREMENTS

In order to test the usefulness of plastic nuclear track detectors in practical situations some measurements were performed utilizing the high energy, ∿250 MeV/nucleon, particle beams now available at the Berkeley Bevatron. First, however, nuclear emulsions were utilized in order to define the particle beam characteristics.

### 1. Ranges of $^{14}N$ Ions in G. 5 Emulsion

The ranges of 99 tracks were measured in an Ilford G.5 emulsion stack exposed at the Bevatron. Several points along each track were measured to obtain the "true" range as well as the projected range. All tracks showing an interaction were systematically excluded.

The distribution in projected range, $R_p$, for all 99 tracks is shown in Figure 10. On this scale the distribution in true range, R, would appear essentially the same and has not been plotted. The peak region ($3.90 < R, R_p < 4.15$ cm) is plotted on a greatly expanded scale for $R_p$ in Figure 11 and R in Figure 12.

The information contained in the range distributions is the central value and the moments about this value. For our purposes, the quantities of interest are the central value and the RMS spread as given by the standard deviation. For gaussian distributions the best estimate of the central value is the arithmetic average. If all 99 measured tracks are included we obtain the following average values for R and $R_p$

$$\overline{R} = 4.004 \pm 0.043 \text{ cm}$$

$$\bar{R}_p = 3.998 \pm 0.043 \text{ cm}$$

and the standard deviations of a single measurements are

$$\sigma_R = 0.430 \pm 0.031 \text{ cm}$$

$$\sigma_{R_p} = 0.430 \pm 0.031 \text{ cm}.$$

Examination of the particle range distributions shows, however, that the above results suffer because of the several ranges which deviate appreciably from the main body of distribution. Only 11 of 99 tracks or 11.1% rather than the expected 31.7% of the particles have ranges greater than one standard deviation from the average. This implies that the distributions are not gaussian and the measured dispersion is contributed mostly by the few largely deviating tracks and does not accurately represent the dispersion of the peak. Thus a better average can be obtained by restricting ourselves to the tracks in the immediate vicinity of the peak. For the 84 tracks in the range $3.90 < R, R_p < 4.15$ cm the average ranges are:

$$\bar{R} = 4.0308 \pm 0.0039 \text{ cm}$$

$$\bar{R}_p = 4.0244 \pm 0.0037 \text{ cm}$$

and the standard deviations of a single measurement are

$$\sigma_R = 0.036 \pm 0.003 \text{ cm}$$

$$\sigma_{R_p} = 0.0338 \pm 0.0026 \text{ cm}$$

Careful examination shows that even these restricted portions of the distributions are non-gaussian. Thus, the final approach to obtaining the true central values of the peaks and the stopping $^{14}N$ beam alone unaltered by nuclear reactions is to fit a gaussian curve through the counts in the three "bins" nearest the

peak. This is accomplished not by taking the average and standard deviation but by fitting

$$\Delta N_i = \left(\frac{dN}{dx}\right)_i \Delta R = \frac{N\Delta R}{\sqrt{2\pi}\,\sigma} \exp\left(-\frac{[R_i - \bar{R}]^2}{2\sigma^2}\right)$$

to the three measured values of $\Delta N_i$ by adjusting the total number, N, the average value, $\bar{R}$, and the standard deviation, $\sigma$. This approach gives:

$$\bar{R} = 4.0237 \pm 0.0018 \text{ cm},$$

$$\bar{R}_p = 4.0200 \pm 0.0014 \text{ cm},$$

$$\sigma_R = 0.0117 \pm 0.0013,$$

and

$$\sigma_{R_p} = 0.0091 \pm 0.0010.$$

This implies an energy of 242.0 ± 0.1 MeV/amu at the entrance face of the emulsion.

It can be seen that the counts in the three central bins around the peak do represent the stopping point distribution due to the $^{14}N$ ions from an almost mono-energetic source which have not undergone nuclear interactions or any other range dispersing interactions other than the range straggling due to the randomness of the randomness of the energy transfers to electrons. For protons of 242 MeV/amu the standard deviation in range due to range straggling is 1.10%. Since range straggling goes inversely as the square root of the atomic number, this implies a 0.295% straggle for $^{14}N$. The values obtained from the three central bins are:

$$\frac{100\sigma_R}{R} = 0.29 \pm 0.03\%$$

and

$$\frac{100\ \sigma_{R_p}}{R_p} = 0.23 \pm 0.02\%$$

The difference between the average "true" range and projected range is also of interest. It can be interpreted in terms of the multiple scattering. Using the average obtained from all 99 tracks

$$\overline{R} - \overline{R}_p = 0.006 \pm 0.061 \text{ cm.}$$

The averages from the restricted range interval, $3.90 < R,R_p < 4.15$ cm., gives:

$$\overline{R} - \overline{R}_p = 0.0064 \pm 0.0054 \text{ cm.}$$

The gaussian fits to the 3 central bin results give

$$\overline{R} - \overline{R}_p = 0.0037 \pm 0.0023$$

Each of these differences implies that to obtain a statistically meaningful difference between the true length and the projected length, many more tracks would have to be taken. Taking tracks individually alleviates this problem by removing the spread due to the energy dispersion and the range straggle. For all tracks with $3.90 < R,R_p < 4.15$) except numbers 67, 17, and 13 which had unusually large values of $R - R_p$) the average value of $R - R_p$ is given by

$$\overline{R - R_p} = 0.00442 \pm 0.00028 \text{ cm.}$$

and the standard deviation of a single measurement by

$$\sigma_{R - R_p} = 0.00254 \pm 0.00020$$

Since $\overline{R}_p = \overline{R} \cos \Theta$, where $\Theta$ is the angle made by the track with the average

track direction,

$$\bar{R} - \bar{R}_p = \bar{R}\,(1 - \overline{\cos\theta}) \simeq \bar{R}[1-(1-\frac{\overline{\theta^2}}{2})] = \bar{R}\,\frac{\overline{\theta^2}}{2}$$

$$\overline{\theta^2} = 2(\frac{\bar{R} - \bar{R}_p}{\bar{R}}) = 0.00220 \pm 0.00014.$$

The RMS value of this angle is

$$\sqrt{\overline{\theta^2}} = 0.0469 \pm 0.0015 \text{ radians}$$

$$= 2.69 \pm 0.09 \text{ degrees.}$$

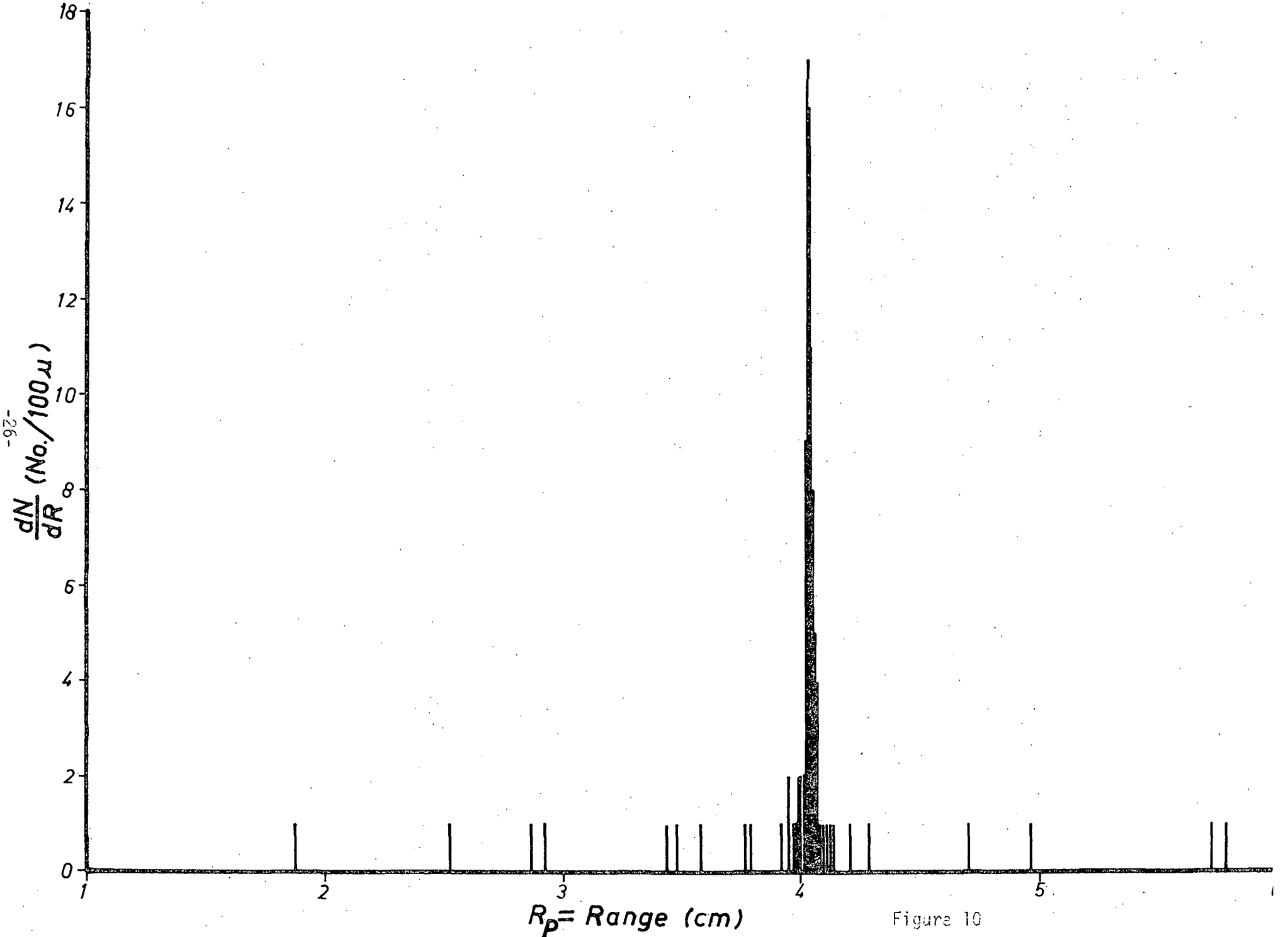


Figure 10

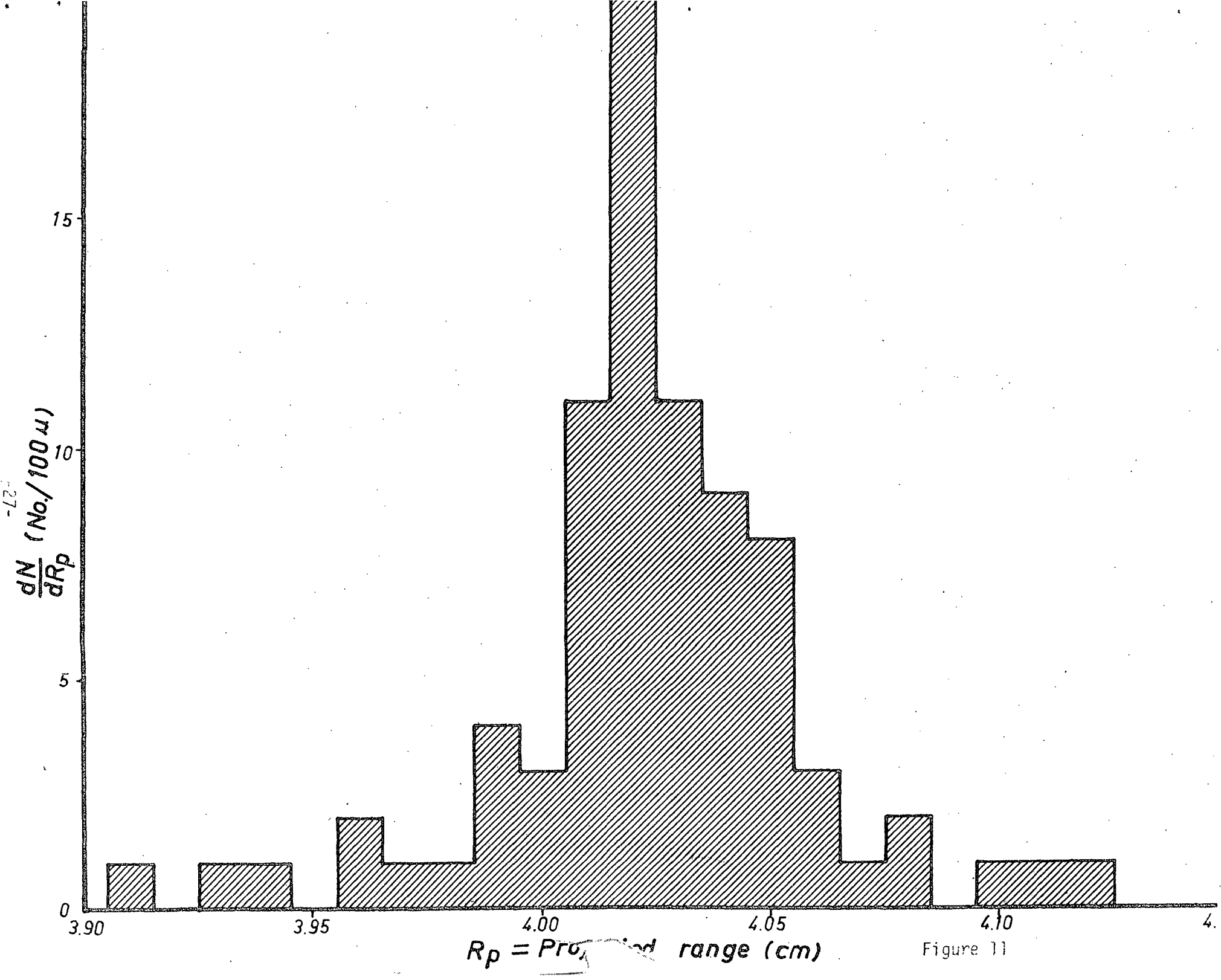


Figure 11

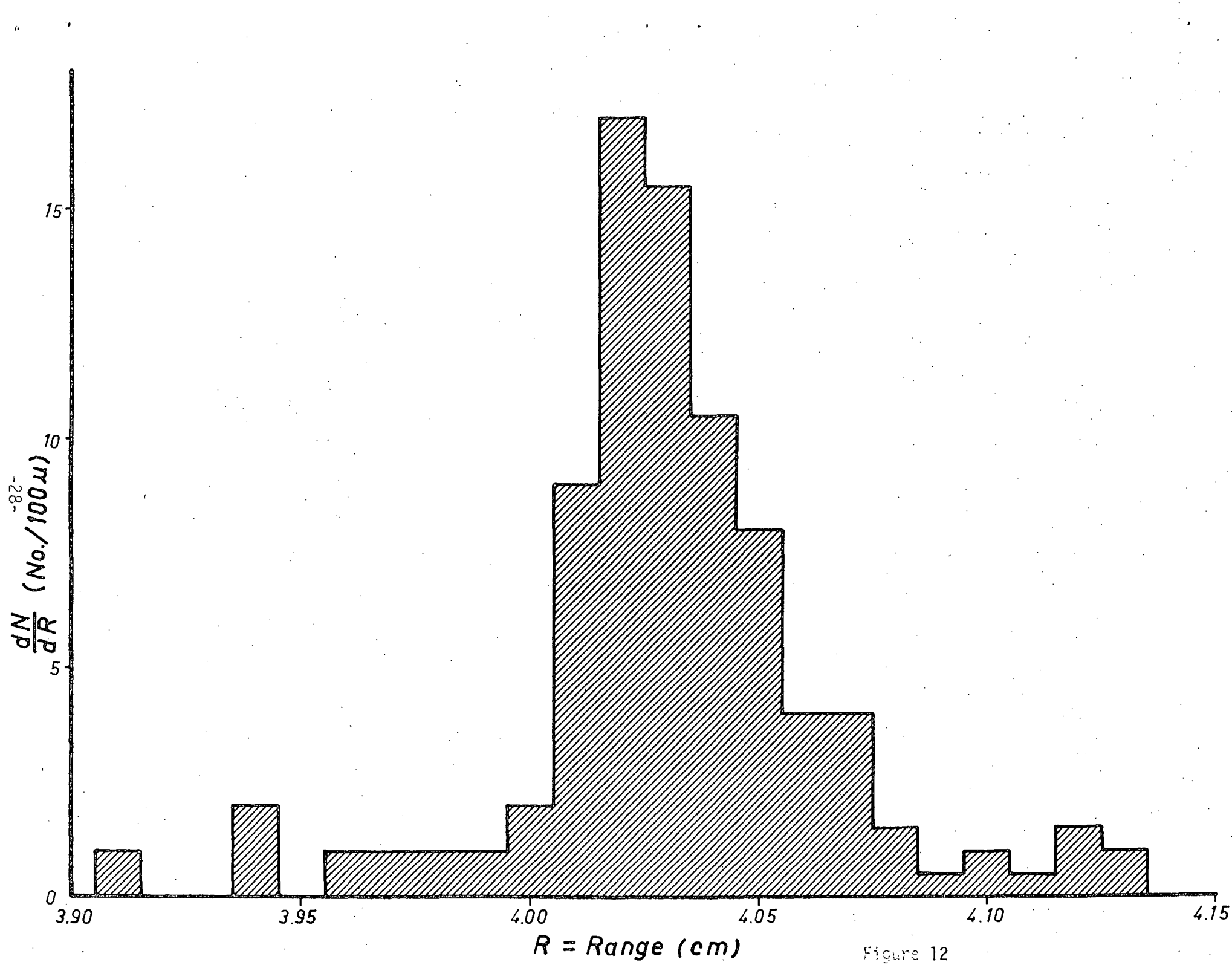


Figure 12

2. Charge Measurements Using Cellulose Nitrate.

Layers of cellulose nitrate, USF #3, detectors were assembled into stacks and exposed normally to the incident ~280 MeV/nucleon, $^{14}N$ ion beam. The incident particle beam was stopped using a 28 layer CN stack (with individual layer thickness of approximately 270 microns) after having been degraded in energy by a 10.6 g/cm$^2$ stack of Lexan. The Lexan degrader thickness was based on the initial expectation of a 250 MeV/nucleon energy beam. Thus only a few straggling particles rather than the expected Bragg peak were stopped in the CN layers.

The detector layers were individually etched at 40°C in 100 ml of 6.25N NaOH. The layer used for locating the stopping point for the particle was etched for 5 hours. The immediately adjacent layer was etched for 2.5 hours, the next for 30 hours, and the last for 48 hours.

The stack configuration and etched track parameters are shown in Figure 13, which is not to scale. The average residual range for each track, $\bar{R}$, is the distance from the stopping point to the center of the etch cone, L. For each track the track etch rate, $V_T$, is given by

$$V_T = \frac{L}{t_e} ,$$

where $t_e$ is the etch time for that layer.

For all the tracks measured $V_T$ has been plotted as a function of $\bar{R}$, as shown in Figure 14. Two groups of points are apparent. One curve has been drawn through the measured points attributed to $^{14}N$ particles. The second group of points represents $^{12}C$ particles (some beam contamination was present). A point from an independent experiment utilizing 10 MeV/nucleon $^{16}O$ particles is also shown as is the bulk etch rate, $V_G = B/t_e$. The bulk etch rate represents the smallest value of $V_T$ possible. From Figure 14 it is noted that $V_T$ is a function of the etch time. This implies a depth dependence of $V_T$ in the detector.

As can be seen from Figure 14, the measured response of the CN detector is such that charge identification of the CNO group of stopping particles is achieved. This charge resolution should be compared with the apparently better resolution indicated in Figures 2, 3 and 4. In fact, the tightness of the points about the lines in Figures 2 and 3 implies isotropic separation might be possible, even for individual particles. The greater dispersion of Figure 14 combining the data from several layers, etched for different lengths of time. This corresponds to the usual situation in which absolute measurements of Z are to be made using calibration data obtained from other sheets of plastic. The smaller dispersion in Figures 2, 3 and 4 indicates that in cases where single sheets of plastic can be internally calibrated, or where single sheets are used for differential measurements, greater accuracy can be obtained than with mixed groups of layers.

As can be seen from Figure 14, the measured response of the CN detector is such that charge identification of the CNO group of stopping particles is achieved. This charge resolution should be compared with the apparently better resolution indicated in Figures 2, 3 and 4. In fact, the tightness of the points about the lines in Figures 2 and 3 implies isotropic separation might be possible, even for individual particles. The greater dispersion of Figure 14 combining the data from several layers, etched for different lengths of time. This corresponds to the usual situation in which absolute measurements of Z are to be made using calibration data obtained from other sheets of plastic. The smaller dispersion in Figures 2, 3 and 4 indicates that in cases where single sheets of plastic can be internally calibrated, or where single sheets are used for differential measurements, greater accuracy can be obtained than with mixed groups of layers.

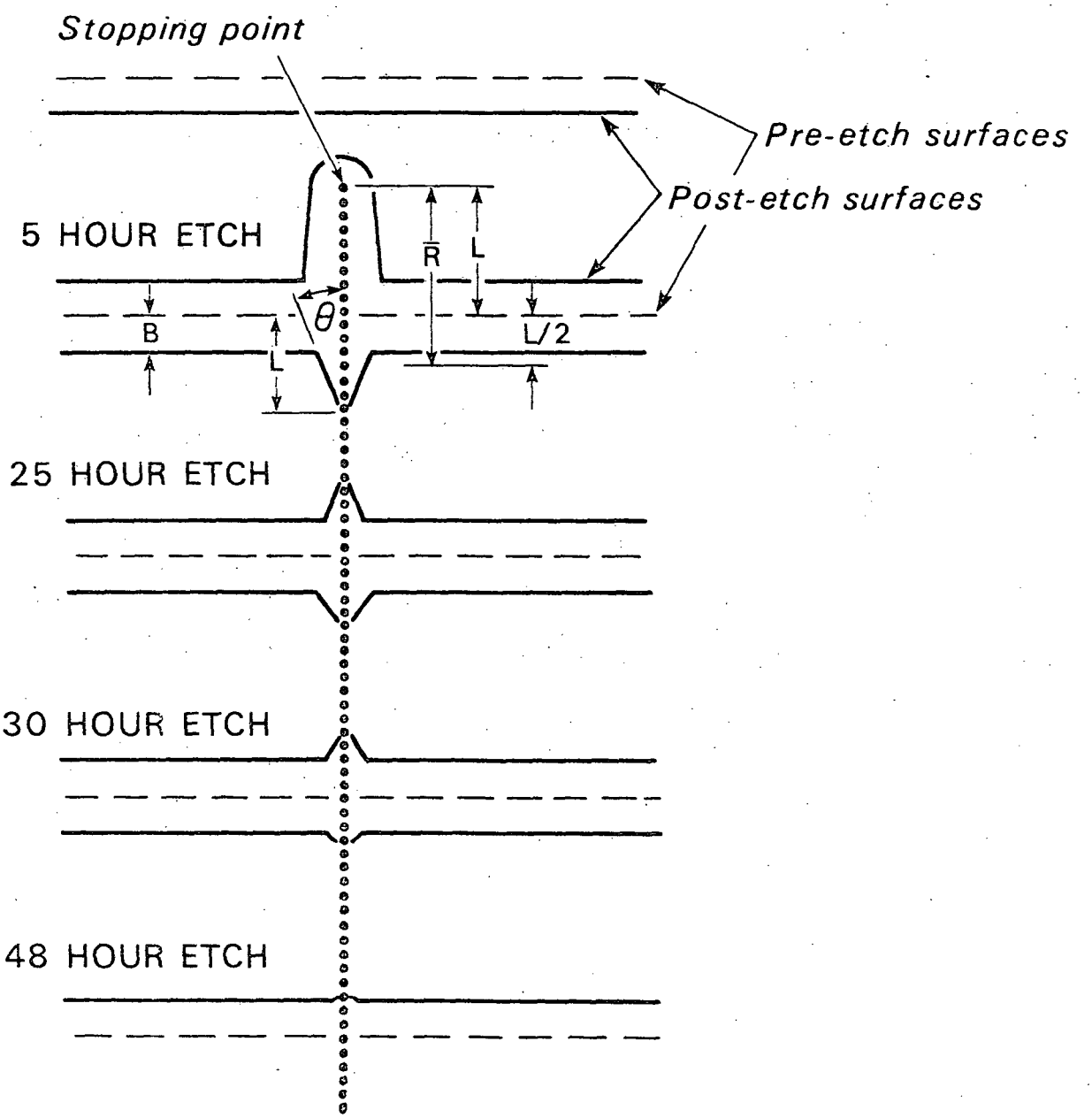
Stopping point
Pre-etch surfaces
Post-etch surfaces
5 HOUR ETCH
R
L
θ
B
L
L/2
25 HOUR ETCH
30 HOUR ETCH
48 HOUR ETCH

Figure 13

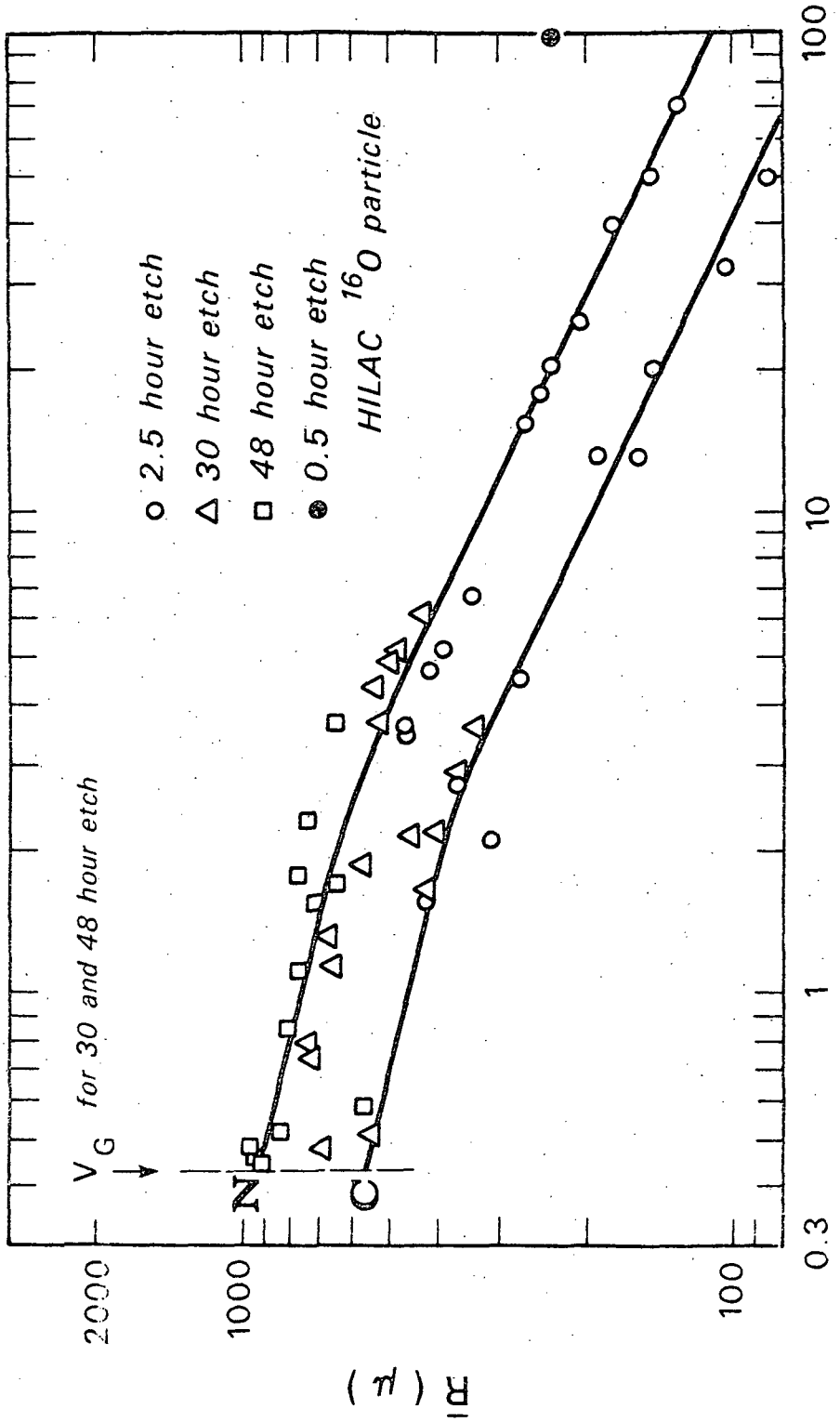
2000
1000
100
0.3
1
10
100
R (μ)
$V_T$ (μ/hour)
$V_G$ for 30 and 48 hour etch
N
C
○ 2.5 hour etch
△ 30 hour etch
□ 48 hour etch
● 0.5 hour etch
HILAC $^{16}O$ particle

Figure 14

3. Bragg Peak Measurement.

A stack of 30 Daicell (red) cellulose nitrate plastics, each 250 microns thick was exposed normally to an incident beam of $^{16}O$ particles. Enough Lexan plastic degrader was added in front of the stack so as to stop the beam roughly in the center of the CN stack. An exposure consisting of a single pulse of 31,154 counts was made. The plastics were then etched for 8.0 hr. at 40°C in 6.25N NaOH solution.

Individual layers were then optically scanned and all stopping particle tracks recorded. The results are shown in Figure 15. The width of the primary peak is apparently primarily the result of the particle range straggling with the initial momentum spread of the particle beam making very little contribution. The subsequent stopping particles are apparently lower charge fragments created in interactions. The experiment clearly showed that plastic detectors are quite useful in mapping the three-dimensional structure of the Bragg peak of heavy particle beams.

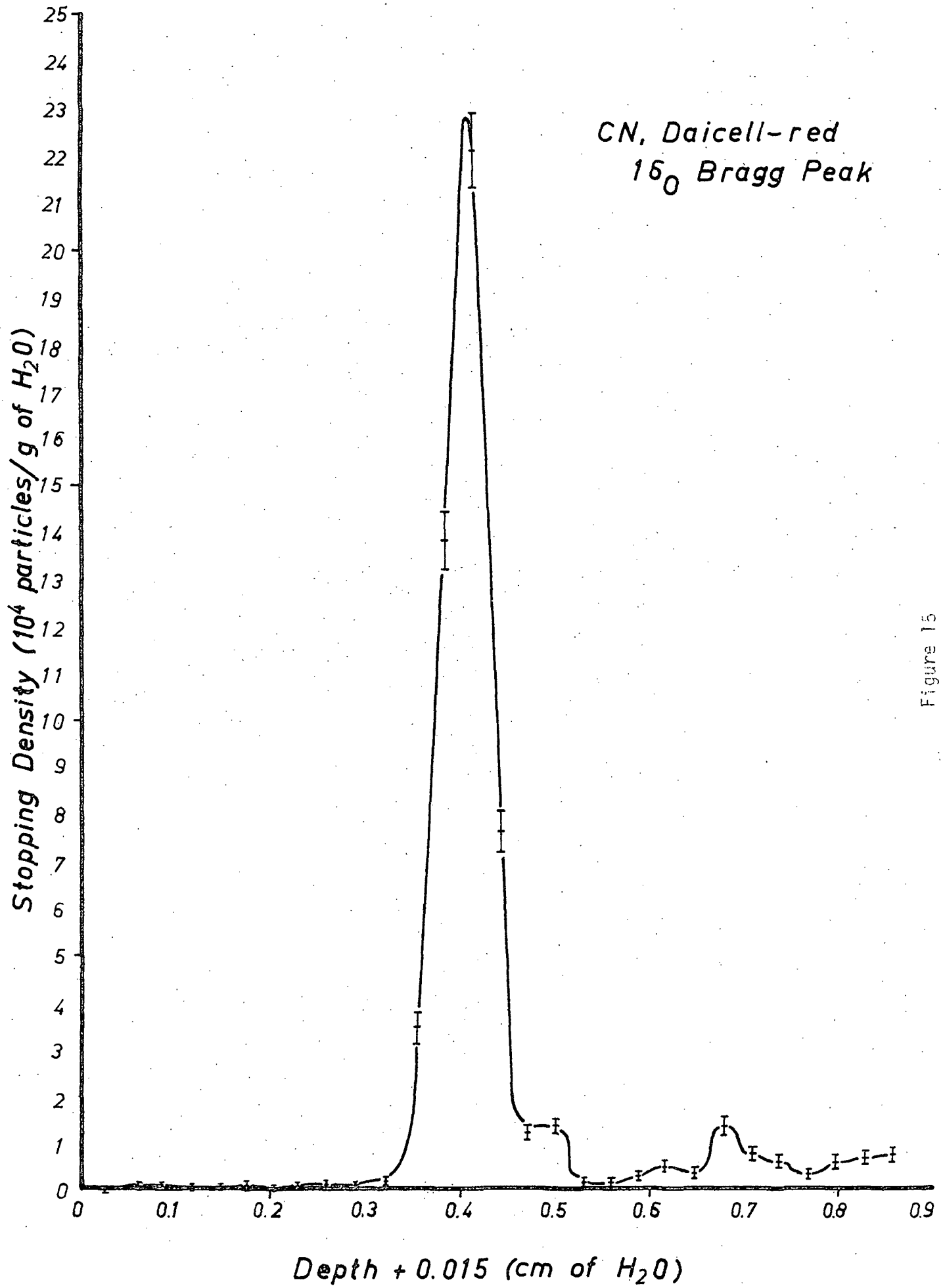
CN, Daicell-red
$16_O$ Bragg Peak
Stopping Density ($10^4$ particles/g of $H_2O$)
Depth + 0.015 (cm of $H_2O$)
0
1
2
3
4
5
6
7
8
9
10
11
12
13
14
15
16
17
18
19
20
21
22
23
24
25
0
0.1
0.2
0.3
0.4
0.5
0.6
0.7
0.8
0.9

Figure 15

## Acknowledgements

The authors wish to thank Dr. H. H. Heckman of the Lawrence Berkeley Laboratory for the loan of the nuclear emulsion stack.

## REFERENCES

1. P. B. Price, R. L. Fleischer, Ann. Review of Nuclear Science, 21, 1971.

2. E. V. Benton, "A Study of Charged Particle Tracks In Cellulose Nitrate," USNRDL-TR-68-14 (1968).

3. R. P. Henke, E. V. Benton, H. H. Heckman, Radiation Effects, 3, 43,(1970).

## Figure Captions

Figure 1. Calibration plot of $V_T$ vs. $\bar{R}(\mu)$ of $^{16}O$ ions in USF 4 cellulose nitrate for a 5.0 hr. etch at 40°C in 6.25N NaOH. Data for both "air" and "metal" surfaces is given.

Figure 2. Calibration plot of $V_T$ vs. $\bar{R}(\mu)$ of $^{16}O$ ions in USF 4 cellulose nitrate for a 20.0 hr. etch at 40°C in 6.25N NaOH. "Air" surface data only.

Figure 3. Same as in Figure 2 except the data is for the "metal" surface. Note the difference from the previous three sets of data.

Figure 4. Calibration plot of $V_T$ vs. $\bar{R}(\mu)$ of $^{20}Ne$ ions in USF 3 cellulose nitrate. Data is from a single surface.

Figure 5. Effect of aging of latent tracks in Lexan as a function of aging atmospheres.

Figure 6. Calibration plot of $V_T$ vs. $\bar{R}(\mu)$ of $^{16}O$ ions in UV-irradiated Lexan processed for 5.0 hr. in a saturated solution at 40°C.

Figure 7. Calibration plot of $V_T$ vs. $\bar{R}(\mu)$ of $^{16}O$ ions in UV-irradiated Lexan processed for 20.0 hr. in a saturated solution at 40°C.

Figure 8. Same as Figure 7 except processed for 100.0 hr.

Figure 9. Etch rate ratio $V_T/V_G$ as a function of $LET_{350}$ for USF 3 cellulose nitrate, UV-irradiated Lexan, non-UV-irradiated Lexan.

Figure 10. Distribution of projected ranges of 250 MeV/nucleon $^{14}N$ particles in Ilford G.5 emulsion.

Figure 11. Same as Figure 10 except the main peak has been enlarged.

Figure 12. Distribution of the true ranges.

Figure 13. Schematic drawing of a processed plastic detector stack.

Figure 14. Charge resolution in USF 3 cellulose nitrate.

Figure 15. The measured Bragg peak of stopping $^{16}O$ particles in cellulose nitrate.